

On the Quest for Oxygen Evolution Reaction Catalysts Based on Layered Double Hydroxides: An Electrochemical and Chemometric Combined Approach

Isacco Gualandi,* Elisa Musella, Giulia Costa, Massimo Gazzano, Erika Scavetta, Sergio Zappoli, and Domenica Tonelli

The oxygen evolution reaction (OER) is a crucial process in various energy conversion and storage technologies, such as water electrolysis. Developing efficient and cost-effective electrocatalysts is essential to achieve the commercialization of devices for the transition toward sustainable energy solutions. Herein, ternary layer double hydroxides (LDHs) are synthesized and characterized as electrocatalysts for OER using a potentiodynamic electrochemical deposition method on Grafoil. A chemometric approach based on experimental design is employed to rationalize the effort in the investigation of the LDHs which are based on Ni, Co, and Fe. The deposited films are characterized using cyclic voltammetry and X-ray diffraction to determine peak currents and potentials, and crystal size. Furthermore, the electrocatalyst performances are assessed by linear sweep voltammetry in 1M KOH from which the Tafel slope and onset potential are calculated. The obtained data are used to derive models describing the material properties and electrocatalyst performance as a function of the electrolyte composition used during the LDHs electrodeposition. This study provides valuable insights into the relationship between the electrocatalyst composition and its OER activity, enabling the design of more efficient and sustainable electrochemical systems for energy applications.

1. Introduction


Today, humanity is facing serious challenges such as environmental pollution, energy crisis, and climate change. In the transition toward the green economy, electrochemical devices are believed to play a key role^[1–5] for storing and converting electrical energy produced by intermeeting renewable power sources. In particular, water electrolysis has drawn a lot of attention since the green hydrogen production has been an efficient way to store the excess electricity produced by photovoltaic and wind power plants. Since oxygen evolution reaction (OER) displays a slow kinetics, OER catalysts must be employed to decrease the required overpotential, which thereby increases the water oxidation efficiency. To handle this issue, a key strategy is the development of electrocatalysts displaying performances like efficiency and ability to deliver high current density, durability, sustainability, nontoxicity, abundance, recyclability, and nonsusceptibility to geopolitical supply risks.^[2] Until now,

noble metal-based materials are the most effective electrocatalysts for OER, but their prohibitive cost and scarcity prevent their large-scale use, and consequently the development of low-cost and efficient catalysts is critical in the implementation of energy grids based on renewable sources.^[4,6–8] In the last decade, first row transition metal oxides and (oxy)hydroxides have gained more and more interest as OER catalysts in alkaline media because of their abundance on earth and low cost. In particular, Ni, Co, Fe, and Mn hydr(oxy)oxides^[9] have been systematically investigated and their OER activities have resulted in the order: Ni > Co > Fe > Mn.^[9]

Layered double hydroxides (LDHs) containing such metals are interesting materials since they display properties such as large surface-to-volume ratio, much more efficient exposure of catalytic active sites in comparison with the 0D and 1D materials, controllable layered structure adjustment (intercalation, topological transformation, and assembly of other functional materials), tunable chemical composition with different cations ratios, hierarchical porosity which facilitates the diffusion of water molecules and release of gaseous products, strong electrostatic

I. Gualandi, E. Musella, G. Costa, E. Scavetta, S. Zappoli, D. Tonelli
Department of Industrial Chemistry "Toso Montanari"
University of Bologna
Via Piero Gobetti 85, I-40129 Bologna, Italy
E-mail: isacco.gualandi2@unibo.it

M. Gazzano
Istituto per la Sintesi Organica e la Fotoreattività (ISOF)
Consiglio Nazionale delle Ricerche (CNR)
via Gobetti 101, 40129 Bologna, Italy

 The ORCID identification number(s) for the author(s) of this article can be found under <https://doi.org/10.1002/aesr.202400233>.

© 2024 The Author(s). Advanced Energy and Sustainability Research published by Wiley-VCH GmbH. This is an open access article under the terms of the Creative Commons Attribution License, which permits use, distribution and reproduction in any medium, provided the original work is properly cited.

DOI: 10.1002/aesr.202400233

interactions between layers and interlayer anions to offer an ordered arrangement of interlayer species, and a tailorable orientation of active sites as well as an increased structural stability.^[10–12] Moreover, incorporation of appropriate defects increases the dangling bonds and decreases the active sites coordination number, resulting in an altered electronic structure and intrinsic electrocatalytic OER activity.^[13] Yet, it remains challenging to solve their poor conductivity, low electron and charge transfer ability, and insufficient active edge sites, especially for the bulk form of LDHs.^[4,9,14–17]

However, LDH-based electrocatalysts have not yet been employed in commercial electrolyzers and their performance in relevant environment is still an open question, which can be addressed by boosting the system further through the incorporation of a third metal within the host layers. The additional metal center can regulate the electronic structures of LDHs resulting in synergistic effects among all metals, thus leading to three-metal LDHs with higher electrocatalytic activities.^[7] Furthermore, the literature has reported the controllable incorporation of Co into Ni/Fe-LDHs to obtain excellent OER electroactivity.^[18]

Nevertheless, a systematic study to find the optimal composition of a three-metal LDH is still missing due to the huge experimental efforts that are requested. To design suitable experiments in order to have a survey among a wide range of possible metals ratios, chemometrics can help. Chemometrics is the science of extracting relevant information from chemical systems. It is interdisciplinary and employs methods frequently exploited by data-analytic disciplines in order to optimize analytical methods and solve problems in applied science, such as (electro)chemistry.^[19] Design of experiments (DOE) is a tool used to systematically evaluate problems which involve too many variables to be analyzed randomly or in a univariate manner. An experimental design approach should be a valuable tool to estimate the influence of different variables on the studied responses and to predict, with a given statistical significance, the effects of each variable and of their interaction on them.^[20]

Hereby, efforts have been devoted for incorporating Co into Ni/Fe-LDH host layers with the aim to modulate their electronic structures and to promote the generation of metal higher valences, thus enriching the active sites and boosting the catalytic activities under the guidance of chemometric tools.

In particular, LDHs have been synthesized through our most recent electrochemical synthetic route based on a potentiodynamic approach.^[21] The procedure rapidly produces deposits of LDH films with high reproducibility (independently of the adopted conductive substrate) and a well-controlled and defined metal ratio,^[22–24] which is highly desirable when the production of considerable amounts of catalysts is needed.

Since the LDH chemical composition is highly tunable by varying several parameters, it is necessary to adopt an efficient approach in the study and the exploration of new electrocatalysts. We decided to apply a DOE strategy to plan the tests necessary to investigate the complex activity features of electrodes modified with three-metal LDHs. Mixture design is a well-known and powerful approach to understand the properties of materials when it is possible to define and control the components of the object to be studied (complete reviews can be found in Leardi^[25] and in the extensive treatments by Cornell^[26] and Myers et al.^[27] The

purpose of such systems is to find a reliable model describing the properties of the material as a function of the varying parameters in all the cases in which the response to a mixture depends on the proportions of the present components and not by the absolute amount of the mixture components. Usually, second- or third-order polynomial canonical models (originally proposed by Scheffé^[28]) are used to find, by regression analysis, the effects of the individual component, called linear blending portion, and of the synergistic or antagonistic blending effect between or among components. In the case under investigation, the mixture is represented by the three metals (Fe, Ni, and Co) present in the LDH which constitutes the electrode modifier. The constrain, as usual, is that the sum of the molar ratios of all components of the mixture must be unity. Summarizing, three-metal LDHs, based on different molar ratios of Fe, Ni, and Co, have been synthesized and characterized following the indications suggested by the chemometric model with the aim to find out the best LDH composition in terms of electrocatalytic performance toward OER, evaluated on the basis of the onset potential and the Tafel plot's slope.

2. Results and Discussion

2.1. Design of Experiments

The compositions of electrochemical baths, which were employed to prepare the OER electrocatalysts, were defined with DOE to minimize the experimental effort and maximize the acquired information. The initially adopted approach was limited to the points D, G, H, K, L, and M (Figure 1). These points are the vertices and the midpoints of the sides of an equilateral triangle and were placed in the area where it was assumed that the materials of the greatest activity would be found. Limiting the study to the points D, G, H, K, L, and M, the obtained models identified the best catalysts among binary LDHs, and this outcome is in contrast with the literature which reports that ternary LDHs

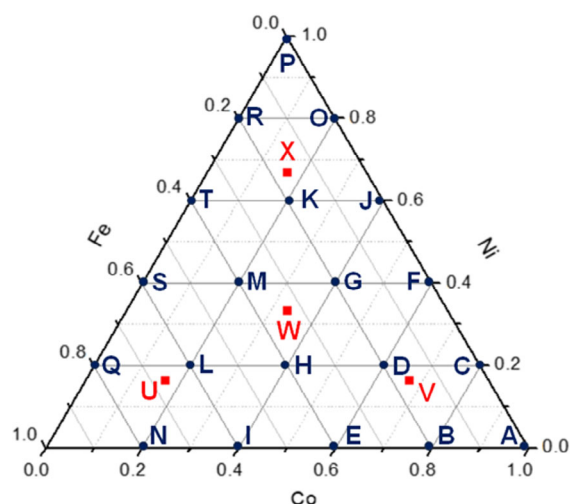


Figure 1. Ternary diagram reporting the compositions of electrochemical baths identified by DOE for the development of the models (blue) and the prediction of the model (red).

should exhibit the best performances. We, therefore, expanded the area under investigation, maintaining the required symmetry around the centroid of the studied compositions.

In Figure 1, the experimental design is reported. It is based, as already said, on a simplex-lattice ternary diagram with a variation of 20% in the molar fraction of each metal. This diagram presents 21 experimental points to investigate but only 20 were studied, as explained before. For three components, the experimental region is represented by a triangle where each of the vertices corresponds to an electrode made with the hydroxide of only one component. The points of the simplex-lattice were used to define the models for the behavior of the electrode. The prediction of the model was checked using electrodes with a composition different from that of any of the points used for the definition of the model. The control points are shown as red square in Figure 1.

A well-known and powerful approach is based on the design of mixtures, by which it is possible to define and control the components of the object to be studied. Our goal is to find a model that can describe the properties of the material as a function of the varying parameters for all the cases in which the response to a mixture depends on the proportions of the components and not by the amount of the mixture components. The investigated models (in SI paragraph) are generally used in the literature^[25–28] to analyze mixtures whose composition presents constraints. Moreover, it was verified that when subsets are selected within the investigated points, following the canonical criteria of the experimental design, it is not possible to obtain models that fully describe the performance of the produced electrocatalysts. This suggests that the high number of the studied points is necessary to have an overall picture of the influence of the composition of the synthesis bath on the properties of the modified electrodes.

2.2. Structural Characterization

To gain details about the structure of the samples, they were submitted to X-ray diffraction (XRD). Although the scans were collected with high data collection times, since the layer of the deposited material is thin (about 1 μm), the patterns show the high reflections due to platinum support. After background subtraction, the LDH structure is revealed by the presence of 003 and 006 reflections that are ascribable to the diffraction by the hydroxide layers. Some examples of XRD patterns are shown in Figure 2. The full set of the XRD, which is reported as SI (Figure S1–S24, Supporting Information), shows that the order of the LDH structures is low since only 003 and 006 reflections, due to layers periodicity, are well evident. It is worth noting that the presence of a LDH phase is confirmed for all the electrocatalysts for which the Fe fraction is equal or lower than 0.6. Moreover, 003 and 006 reflections are split in the range of compositions with high Co percentages (Co100, Co80Fe20, Co60Fe40), so proving the contemporary presence of two LDH phases for those materials. From the positions of reflections on the 2-theta scale and from their width, the interlayer distances (d_{003}) and crystallite sizes were, respectively, calculated and plotted in Figure 3. Figure 3A shows the experimental ternary diagram of the interlayer distances as a function of LDH composition. The d_{003} values are comprised between 7.68 and

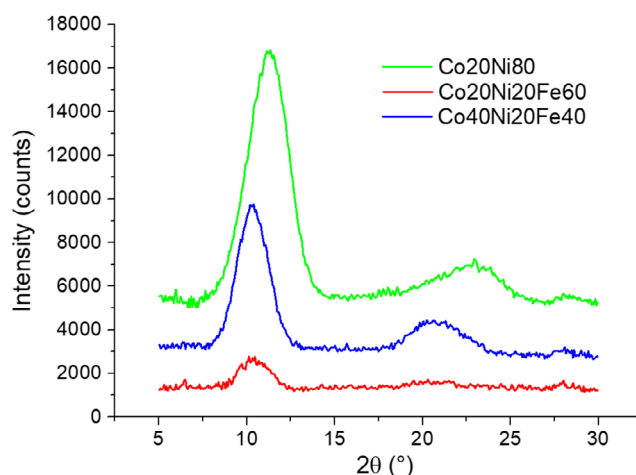


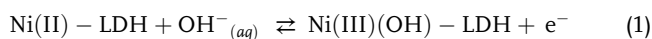
Figure 2. XRD spectra of three selected LDH samples.

9.00 \AA . The two areas colored in blue exhibit the lowest interlayer distances ($<8.00 \text{\AA}$) and are placed where the content of Ni or Fe is close to 1. The d_{003} highest values ($>8.67 \text{\AA}$) are observed for the binary Ni40Fe60 and CoNi LDHs with a high fraction of Co. The area colored in gray, with a Fe fraction equal or higher than 0.8, represents the composition where the 003 and 006 reflections of LDH structure were not found. Consequently, the absence of the signals relevant to LDH phases suggests that they were not obtained, likely due to a Me(II)/Me(III) ratio in the deposition bath that deviated significantly from the typical values required for LDH structures. Additionally, the presence of inhomogeneous films on the electrode surface indicates the deposition of amorphous materials, which were not detected by XRD. Figure 3B reports the ternary diagram of crystal sizes as a function of LDH composition. The values range between 28 and 69 nm. The highest values (>59) are found in the area colored in red or orange and which is characterized by the highest Co fraction. On the other hand, the lowest values (blue) are placed in the zones with a high fraction of Fe or Ni. Summarizing the presence of Co leads to LDHs with both high crystal sizes and interlayer distances. On the other hand, both low interlayer distances and crystal sizes are observed for the compositions with Fe or Ni fraction close to one.

2.3. Electrochemical Characterization

Figure 4 shows the cyclic voltammetries (CVs) characterization recorded in 0.1 M KOH solution at the Grafoil electrodes coated by NiFe LDH, CoFe LDH, and CoNiFe LDH.

For the Ni80Fe20 LDH, the typical peaks, observed at the formal potential of 0.422 V (the average of anodic and cathodic peak potentials), are related to the quasi reversible behavior of the redox couple Ni(III)/Ni(II), involved in the reaction



The formation of the γ phase during the oxidation of Ni(II) centers to Ni(III) leads to a partial irreversibility in the CV response,

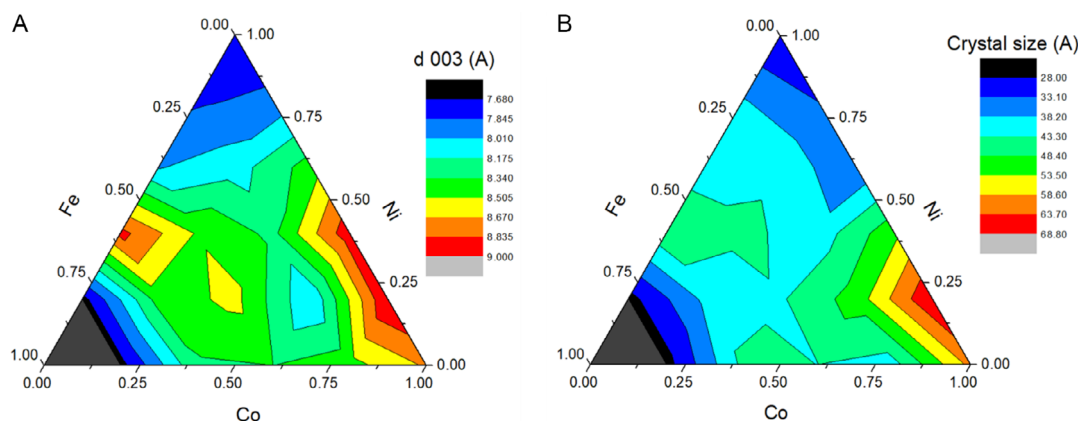


Figure 3. Experimental ternary diagram reporting A) d_{003} and B) crystal size as a function of the composition of the electroynthesis bath.

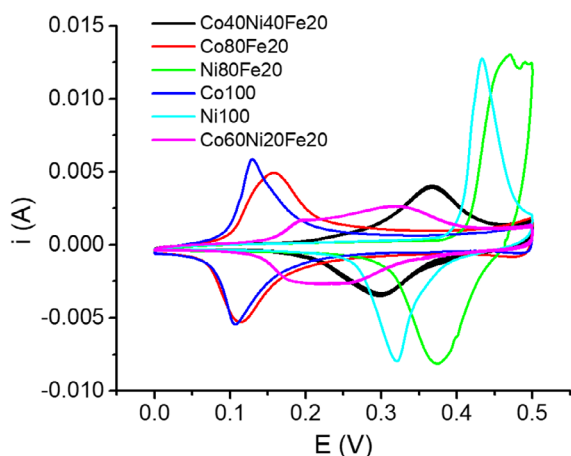
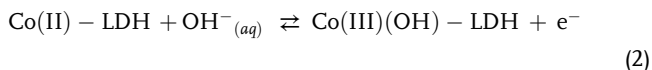


Figure 4. CV recorded in 0.1 M KOH at the Grafoil electrode modified with $\text{Ni}(\text{OH})_2$, $\text{Co}(\text{OH})_2$, and with LDH having different compositions.

as suggested also by a peak to peak separation (ΔE_p) equal to 98 mV.

The Co80Fe20 LDH displays a typical Faradaic and reversible redox wave at about 0.136 V and a capacitive component up to ≈ 0.2 V. The redox wave exhibits a good reversibility ($\Delta E_p = 45$ mV) which can be ascribed to the electrochemical process



When the CVs of NiFe and CoFe-based LDHs are compared with the CVs recorded for the pure hydroxides $\text{Ni}(\text{OH})_2$ or $\text{Co}(\text{OH})_2$ in the alpha phase, it can be observed that the presence of Fe leads to an increase in the formal potential of the Me(III)/Me(II) couples. In particular, the potential shift of the Ni(III)/Ni(II) couple (45 mV) is higher than the one of the Co(III)/Co(II) couple (18 mV). Probably, the presence of the trivalent iron into the structure hinders the extraction of electrons from the Me(II) sites due to the greater positive charge of the LDH layers. Regarding the kinetic factors, it is worth noting that the presence of Fe has a

different effect for Co- and Ni-based materials. The differences between the values of anodic and cathodic peak potential (ΔE_p) are 23 and 45 mV for Co α hydroxide and Co80Fe20 LDH, respectively, highlighting a worsening of the reversibility due to the presence of iron. In reverse, the ΔE_p values found out for Ni hydroxide and Ni80Fe20 LDH are 112 and 98 mV, suggesting that iron improves reversibility for Ni-based systems.

The behavior of films containing Co, Ni, and Fe is intermediate between NiFe LDHs and CoFe LDHs. For most synthesized LDHs, it is like that reported for Co40Ni40Fe20 LDH (Figure 4), in which there is a single redox wave whose formal potential value (0.333 V) is placed between Co80Fe20 LDH (0.136 V) and Ni80Fe20 LDH (0.422 V). This result suggests that Me (II) sites behave similarly throughout the material, regardless of their nature. Some CVs have a more complex shape since shoulders appear, thus suggesting different behaviors of the various Me(II) sites in the material. The CV of Co60Ni20Fe20 LDH is an example for which the behavior is very marked. The anodic peak potential (E_p) and anodic peak current (I_p) values were determined from the CVs recorded for all the synthesized LDHs (Figure S25–S48, Supporting Information) and reported in Table S2, Supporting Information.

Figure 5A presents a ternary diagram illustrating the trend of E_p as a function of hydroxide composition. The highest E_p values, ranging from 0.45 to 0.52 V, are observed in compositions with high Ni and low Co content, indicated by the red and yellow regions of the diagram. Conversely, the hydroxides exhibiting the lowest E_p values (between 0.12 and 0.20 V) are found in the area where the cobalt fraction ranges from 0.50 to 1.00 and the nickel fraction spans from 0.00 to 0.45, represented by the blue and light blue regions in the ternary diagram. The CVs of some hydroxides do not allow the extraction of the E_p and I_p values because either the peak was not visible in the applied potential range, or the distribution of the hydroxide film was not homogeneous enough to give a reliable result. This failure is due to a pseudocapacitive behavior of the LDH film, with the absence of an evident redox wave or the peak overlapping with the wave of oxygen evolution reaction. The gray area in the ternary diagram represents the composition range wherein it was not possible to estimate E_p and I values. Figure 5A illustrates that the pure cobalt hydroxide exhibits the lowest anodic

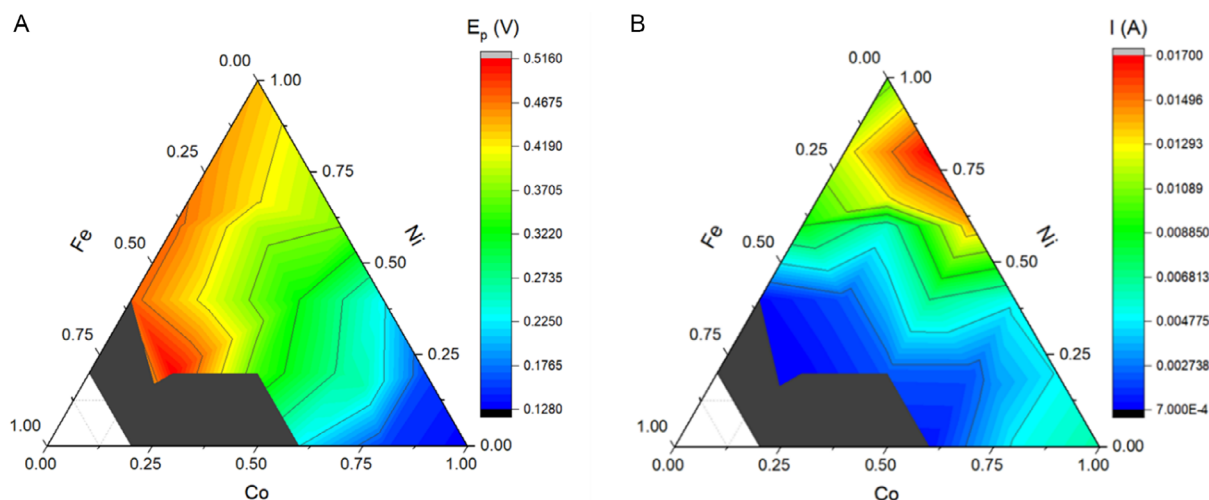


Figure 5. Experimental ternary diagram reporting A) E_p and B) I_p as a function of the composition of the electrocatalysis bath.

E_p values, whereas the highest values are observed in the nickel/iron binary compositions. Transitioning from the region with elevated Ni content to the area with increased Co content, a gradual decrease in the E_p values is observed, suggesting that the behavior of the hydroxide may be represented as a weighted average of the contributions from the two divalent metals.

Figure 5B is the ternary diagram, showing the trend of the I_p as a function of the composition of the hydroxides. In this graph, the gray area indicates the compositions for which the extraction of I_p values was not feasible. Figure 5B reveals that the lowest peak current values, ranging from 0.7 to 5 mA (depicted in the blue region of the diagram), correspond to compositions characterized by a high Fe fraction and a low Ni fraction. In the upper part of the graph, red in color, the highest I_p values are located, approximately between 13 and 17 mA, which refer to a higher Ni content, compared to Co and Fe contents, with a compositional fraction ranging from 0.60 to 0.90. From the two figures, the following considerations can be drawn. The highest I_p values occur for a high content of divalent metals. The increase of the trivalent metal content causes a decrease in the peak current and this result agrees with the presence of a lower quantity of electroactive sites. Furthermore, a high Co content allows for a more reversible electrochemical response.

2.4. OER Performances

Linear scan voltammetry was employed to investigate the kinetic and thermodynamic performances of the synthesized LDHs as OER electrocatalysts. **Figure 6A** shows a typical linear sweep voltammetry (LSV) response recorded in 1.0 M KOH. It can be observed that the current takes on a very low value for potentials comprised between -100 and 280 mV. In this region, the plot appears as a straight line suggesting a capacitive behavior. By moving toward more anodic potentials, a redox wave (C), which can be attributed to the abovementioned oxidation processes involving Me (II), is observed. Finally, at very anodic potentials (D) a marked increase in the recorded current is observed, which

is related to the water oxidation process, and therefore, to OER. The data extracted from the LSVs are the onset potential (E_{onset}) and the Tafel slope which are reported in Table S2, Supporting Information file.

The E_{onset} is the potential at which the OER begins to run and is determined by identifying the potential at which the current begins to gradually increase. The lower the onset potential, the better the performance of the electrocatalyst for OER. All the E_{onset} of the investigated LDHs modified electrodes were plotted to obtain an experimental curve (Figure 6B).

Figure 6B shows that the external edges of the ternary diagram, corresponding to the hydroxides with binary composition, display the highest values (red and green areas) of the E_{onset} , so demonstrating that the ternary hydroxides exhibit a better performance. The area containing the lowest onset values refers to a composition characterized by a high Co content (0.40–0.75). The composition that shows the lowest potential is Co₆₀Ni₂₀Fe₂₀ with a value equal to 1.469 V. It is worth noting that the catalysts with the best performance possess the typical Me(II)/Me(III) ratio usually found for LDHs, that is, between 5 and 1.

The Tafel slope values provide valuable information on the OER kinetics. The lower the value of the slope, the faster the reaction leading to the evolution of oxygen will proceed and the better the performance of the OER catalyst will be. Tafel slope values obtained for the Grafoil electrodes coated by the different LDHs are reported in Figure 6C.

Figure 6C shows that the highest values of Tafel slopes are found in the area close to the edge of binary NiFe LDH where there is a low Co content. Moreover, high slope values are located corresponding to a Ni content higher than the other two metals.

Instead, the areas marked with the blue color represent the lowest values. They are mainly concentrated in the central part of the ternary diagram in correspondence to a 2:1 total Me(II)/Me(III) ratio, and where the Co quantity is higher than Ni and Fe ones. These data suggest that the presence of Co is fundamental to establish an efficient electrode kinetics, and the effect can be explained by analyzing the reversibility of the voltammograms.

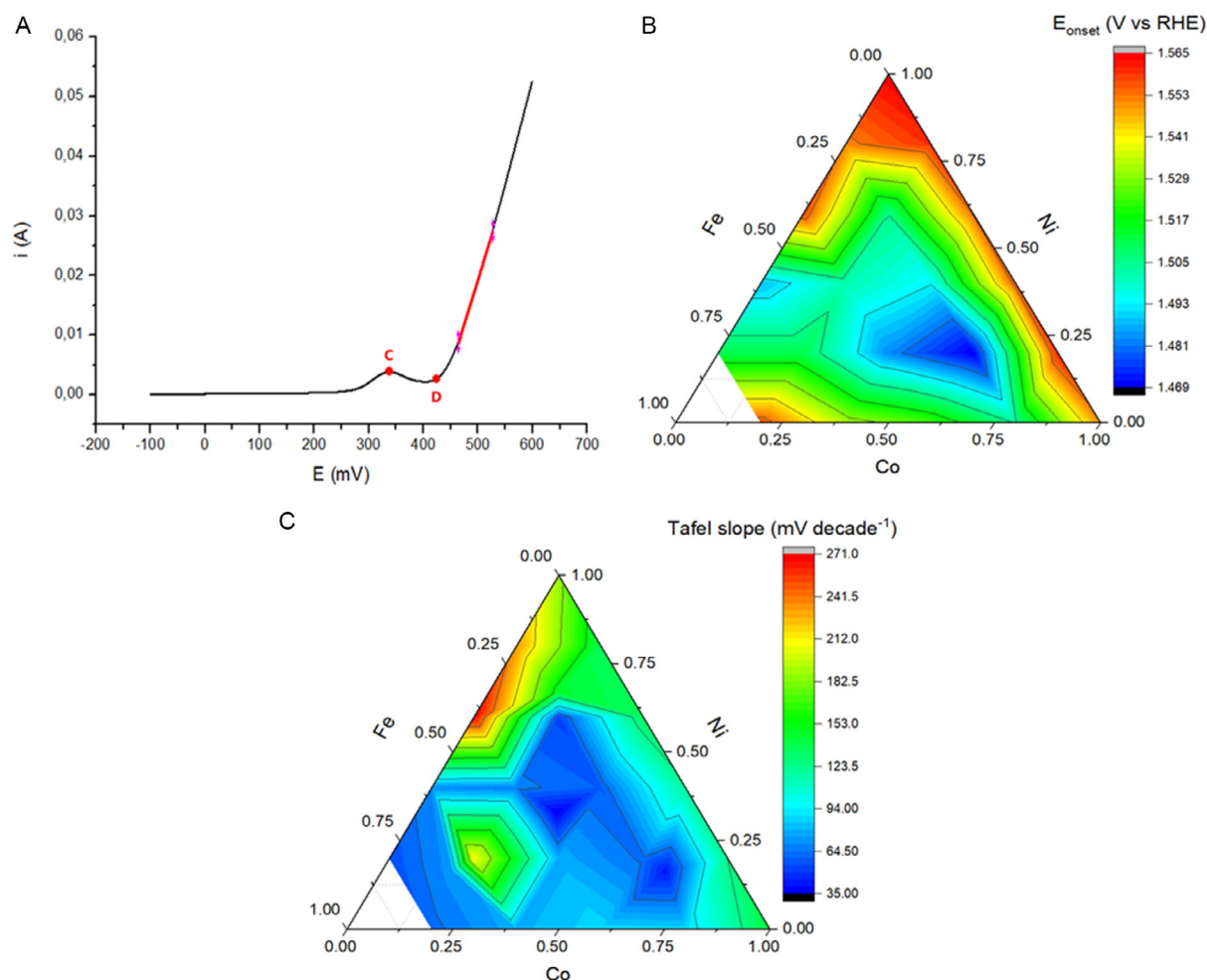


Figure 6. A) Typical LSV recorded in 1.0 M KOH. Experimental ternary diagram reporting the E_{onset} B) and Tafel slope C) as a function of the composition of the electrosynthesis bath.

Hydroxides with a high Co content exhibit better reversibility of the electrochemical process.

2.5. Data Analysis and Model Development

The chemometric elaboration of the data was carried out in order to: 1) identify the correlations among the variables (fractions of Ni, Co, and Fe) and among the various factors (E_p , I_p , crystal size, E_{onset}); 2) identify the weight of the variables on the variability of the factors; and 3) create models that describe the trend of the factors as a function of the metal fractions present in the electro-synthesis bath. All the employed data are reported in Table S2, Supporting Information.

Table 1 shows the correlation coefficients between the variables and the factors, in which the values in bold indicate a correlation significance greater than 95%. The E_p values show a very high negative correlation with the Co fraction, and a significant positive correlation with the Ni fraction. These data are in agreement with the potentials of the Co(III)/Co(II) (lower) and Ni(III)/Ni(II) (higher) couples and with the intermediate behavior

Table 1. Correlations expressed as R value among the fraction of each metal in the material and the experimental parameters. In bold are evidenced significant correlations ($p < 0.05$). $N = 14$; missing data were not considered.

Metal	Tafel slope	E_{onset}	I_p	E_p	Crystal size
Co	-0.20	0.10	-0.14	-0.96	0.65
Ni	0.54	0.44	0.68	0.62	-0.61
Fe	-0.42	-0.72	-0.69	0.52	-0.12

displayed by the hydroxides containing both ions. At the same time, I_p is positively correlated with the Ni(II) fraction and negatively with the Fe(III) fraction. Also in this case, the higher intensity of the current due to Ni(III)/Ni(II) couple compared to the Co(III)/Co(II) couple, and the fact that Fe(III) is not electroactive clearly explains the observed correlations, which are perfectly consistent with the electrochemical behavior (see characterization CVs, Figure S25–S47, Supporting Information). However, the correlation of variables with other parameters can be useful

to find out relationships that are not easily identifiable with a simple analysis of the results. In particular, a negative correlation between the E_{onset} and the Fe fraction is observed, indicating how Fe(III) plays a key role for the improvement of the electrocatalytic performances in the OER reaction, as already reported in the literature^[29] for the Ni-based LDHs. At the same time, the size of the crystals exhibits a significantly positive correlation with the Co fraction and a significantly negative correlation with the Ni fraction, suggesting that for the adopted synthesis conditions, the presence of Co leads to larger crystals, while the presence of Ni leads to smaller ones.

As to the correlations between the parameters, the highest R value is found for Tafel slope and E_{onset} , highlighting how (Table S3, Supporting Information) the preparation of a good electrocatalyst must not require a compromise between the two responses. This result suggests that the kinetic factor dominates both the Tafel slope (which is a purely kinetic parameter) and the E_{onset} through the overvoltage contribution. The values of E_{onset} and, less significantly, of Tafel slope exhibit a negative correlation with the I_p values. Considering that an increase in the E_{onset} and Tafel slope values indicates a worsening of the electrocatalytic performance, this result would suggest that the electrocatalysts displaying the lowest I_p show better performance. However, these results can be explained considering that I_p , E_{onset} , and Tafel slope have a negative correlation with the

fraction of Fe, and, therefore, they are positively correlated to each other. Similarly, the correlation observed between the crystal size and E_p can be explained by the correlation that both parameters display with the Co fraction.

Starting from the negative correlation existing between E_{onset} and Fe fraction, a deeper processing of the data was carried out in order to identify the effect of the variables on E_{onset} and Tafel slope. In particular, **Figure 7A** shows the trend of E_{onset} as a function of the Fe fraction. The points reported in the graph have been grouped and displayed with different colors for the different fractions of Ni. It can be observed that the trend of all the data with constant Ni fraction exhibits a minimum (best electrocatalyst performances), which is always placed at a Fe fraction equal to 0.20. The E_{onset} values for the materials that do not contain Fe range between 1.55 and 1.57 V, highlighting the key role of Fe for the OER electrocatalysts. Considering only the Fe-containing materials, it can be observed that the series of points with fixed Ni composition appear as almost parallel lines, highlighting a poor interaction between these two variables, at least as far as E_{onset} is concerned.

A similar elaboration of data was carried out by plotting the E_{onset} values as a function of the Ni fraction and grouping them for a fixed fraction (Figure 7C). In this case, it can be noticed that: 1) the series of points with Fe fractions equal to 0 exhibits high E_{onset} values regardless the Ni fraction; 2) the series with Fe

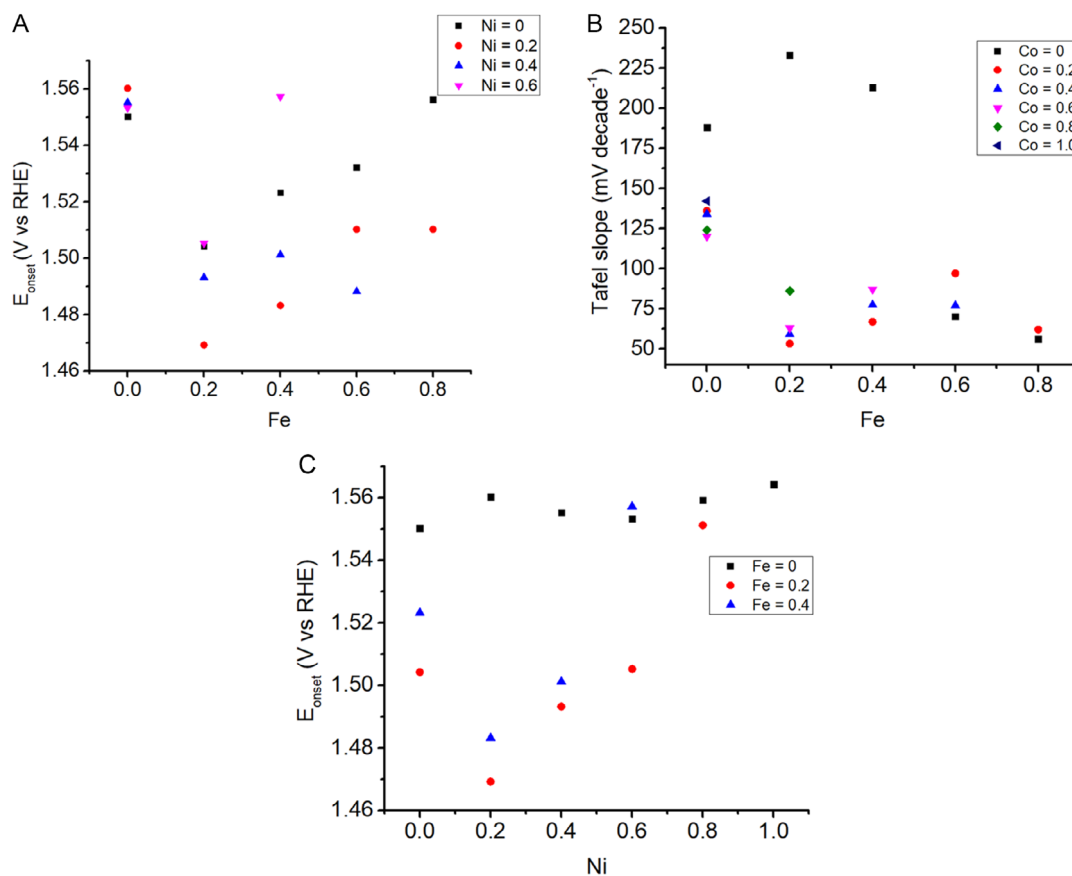


Figure 7. A) E_{onset} versus Fe fraction for different Ni contents; B) E_{onset} versus Fe fraction for different Co contents; and C) Tafel slope versus Ni fraction for different Fe contents.

fraction equal to 0.2 and 0.4, which, therefore, present a significant number of points, exhibit a trend with a minimum (best electrocatalysts) placed at a Ni fraction equal to 0.2. Also in this case, the data series of Fe-containing electrocatalysts usually have a parallel trend, highlighting a low interaction between the Ni and Fe fractions. It is worth noting that the data elaboration as a function of the Co fraction was not significant and an evident trend for the E_{onset} was not visible.

On the other hand, the Co fraction has a more significant effect on the Tafel slope. When the Tafel slope values were plotted as a function of the Fe fraction, all the points were grouped on a single curve, except for three of them which have a Co fraction equal to zero (Figure 7B). The Tafel slopes of this series (Ni100, Ni80Fe20, Ni60Fe40) display the highest values among all the investigated electrocatalysts, suggesting that the presence of Co plays a key role in dictating the kinetics of the overall electrochemical process. The trend of the points for which Co is present shows a maximum of the Tafel slopes at a Fe fraction equal to 0, with a minimum when the Fe fraction is 0.2. However, the curve reaches a maximum at a fraction equal to 0.6, and again decreases at a fraction equal to 0.8.

Summarizing, a deeper data processing highlights that the presence of Fe plays a role in the OER process. It also suggests that the optimal Fe fraction is 0.2 in order to have the best performance in terms of E_{onset} and Tafel slope. Furthermore, the electrocatalysts that display the best E_{onset} values generally have a Ni fraction of 0.2. Co appears to have the effect of a diluent on the E_{onset} response, while it appears important to obtain low Tafel slopes and, therefore, a good charge transfer. The best electrocatalysts are found around the composition Co60Ni20Fe20. Considering the distance of the points in the experimental design, we can say that the uncertainty in identifying the catalyst with the best performance is ± 0.2 for the Fe and Ni fractions.

Moreover, analyzing the Pareto charts of the standardized effect, it is possible to observe that each metal has a different relative weight, hence a different effect, on the response. For all the responses, the mixed effects are negligible with respect to the direct effect of one or more metals. As it is possible to notice (Table S3, Supporting Information section), the percentage of a single metal dominates the observed responses and the sum of the standardized effect of the metal is always above 80%. Therefore, even the Pareto charts show little interaction among the variables for each investigated parameter (Figure S49–S53, Supporting Information).

Finally, the obtained data were used to develop models that describe the trend of E_p , I_p , crystal size, E_{onset} , and Tafel slope as a function of the Ni, Co, and Fe fractions. The functions were chosen between the model reported in the SI in order to obtain the best fit, which is indicated by the p value, with the lowest complexity. All equations describing the model are shown in Table 2, while the surfaces are reported in Figure S54–S57, Supporting Information.

ANOVA conducted on the model prediction, shows that the models are reliable to describe the relationships between the material composition and its activity. The correlation among predicted and observed values are quite satisfying. Table 2 reports the p values resulting from ANOVA, and the intercept, slope, and R^2 values resulting from the linear correlation between the predicted and the experimental values. Furthermore, the predictive capabilities of the models were evaluated using four verification points, chosen in the central part of the ternary graph, and indicated (in red) in Figure 1. The comparisons between predicted and experimental values are reported in Table S4–S8, Supporting Information, for the four verification points.

From the p data of ANOVA, intercept, and slope, we can observe that the model for E_p has the best predictive capabilities. The prediction capacity is also demonstrated by the good ability

Table 2. Statistical parameters and model coefficients of fitting functions. Statistical parameters for the observed and predicted responses (Fe, Ni, and Co are identified by their molar fraction, instead the capital letter A, B, and C are identified as the coefficients reported in the table).

Response	Tafel slope	E_{onset}	I_p	E_p	Crystal size
Useful points (df)	20	20	15	16	18
Df for regression	7	7	6	6	6
Function ^{a)}	Special cubic	Special cubic	Quadratic	Quadratic	Quadratic
ANOVA	$p = 0.006$	$p = 0.009$	$p = 0.012$	$p = 0.000003$	$p = 0.003$
Slope	0.708	0.883	0.759	0.950	0.742
Intercept ^{b)}	31.3	0.18	0.002	0.017	11.3
R^2	0.708	0.686	0.759	0.950	0.742
A	131	1.55	0.00513	0.0941	63.4
B	199	1.56	0.0143	0.450	26.5
C	8.11	1.51	-0.0132	0.754	52.9
AB	-208	-0.0192	-0.000236	0.126	6.37
AC	77.5	-0.0246	0.0133	-0.400	-72.1
BC	182	-0.0530	0.0159	-0.457	22.6
ABC	-1707	-1.40	-	-	-

^{a)}Special cubic function: $f_c = A * Co + B * Ni + AB * Co * Ni + AC * Co * Fe + BC * Ni * Fe + ABC * Co * Ni * Fe$ ^{b)}Quadratic: $f_q = A * Co + B * Ni + AB * Co * Ni + AC * Co * Fe + BC * Ni * Fe$

to predict the verification points, with errors varying between 26 and 40 mV, only slightly higher than the experimental error, which can be estimated at around 10 mV.

When the comparisons between predicted and experimental data were performed with ANOVA or a linear regression, the validity of the other models appears equivalent. The model for E_{onset} results the most promising for the prediction of the verification points behavior, with an error between 3 and 18 mV, in line with the experimental error. The slope values close to 1 and the intercept (0.180) confirm the general validity of the model; however, the lower value of R^2 and the high probability of ANOVA (0.009) highlight a nonoptimal fitting. From the comparison of the model with the experimental values, which exhibit an irregular trend, it could be hypothesized that the fitting curve is not able to best simulate the local variability observed for the individual points, even if it is able to simulate the general behavior of the system.

The greatest error of the models in the prediction of the verification points occurs for the Tafel slope and the I_p . While the ANOVA tests and the R^2 values for the Tafel slope suggest the validity of the model with values of 0.006 and 0.7076, respectively, the intercept value of 31.3 suggests a nonoptimal fitting. Observing the experimental data, the trend of the Tafel slopes is more complex than the ones displayed by the other parameters since it displays two zones with maximum points and two zones with minimum points.

2.6. Study of OER Process for Co60Ni20Fe20

The performance of Co60Ni20Fe20 was examined in greater detail through additional LSV, long-term stability tests, and electrochemical impedance spectroscopy (EIS). Figure 7A displays the LSV recorded for the catalyst across the entire available potential range, achieving current density values exceeding 100 mA cm^{-2} . The overpotential values at current densities of 10 and 100 mA cm^{-2} were found to be 0.275 and 0.322 V, respectively.

Figure 7B illustrates the potential profile recorded while the catalyst was employed in the oxygen evolution reaction, maintaining a current density of 10 mA cm^{-2} . The potential is reported with respect to the reversible hydrogen electrode (RHE), without any correction for the ohmic drop. From the

presented data, it is observed that after an initial phase, in which presumably the complete charging of the materials constituting the electrocatalyst takes place, the electrode stabilizes at a potential of 1.63 V, which remains constant for the subsequent 12 h. These results demonstrate the high operational stability of the catalyst under working conditions.

EIS is a valuable tool to investigate the overall electrochemical process under OER conditions.^[30–32] Figure 7C illustrates the Nyquist plots recorded at: 1) working potentials where the oxygen evolution reaction occurs at a very slow rate (1.367, 1.418, 1.447, 1.459 V vs RHE); 2) the onset potential (1.469 V); 3) the potential corresponding to a current density of 10 mA cm^{-2} , as observed in LSV (1.507 V); and 4) the potential corresponding to a current density of 100 mA cm^{-2} , as observed in LSV (1.552 V).

The data presented in Figure 7C reveal that at lower potentials, the Nyquist plot displays two semicircles, indicating that two distinct electrochemical processes may influence the overall reaction kinetics. The equivalent circuit used for data fitting is depicted in Figure S58, Supporting Information. The first element, represented by R1 and C1, corresponds to the interface between Grafoil and LDH, associated with the semicircle at high frequencies. R2 represents the charge transfer within the LDH film. The second element, consisting of R3 and C2, is related to the charge transfer at the interface between LDH and the electrolyte, represented by the semicircle at lowest frequencies. Finally, R4 is linked to the resistance of the electrolyte.

The fitting results are summarized in Table S9 and Figure S59, Supporting Information, showing the comparison between some experimental and simulated curves. R4 maintains a constant value of 2.1Ω , indicating that it accurately reflects the electrolyte resistance. R2 consistently holds a value of 0.001Ω . Notably, R3 decreases when the potential increases, ranging from an estimated value of 101Ω at 1.367 V to $\approx 0.0601 \Omega$ at 1.552 V. This behavior is consistent with an increase in the rate of the oxygen evolution reaction as the applied potential rises. Concurrently, R1 also decreases with the increase of the applied potential, suggesting enhanced charge transfer between Grafoil and LDH at higher potentials.

Interestingly, the decrease in R1 when the potential increases is less pronounced than that of R3. The measured values indicate that at potentials below the onset, R1 is lower than R3, implying that the overall rate of the electrochemical process is primarily

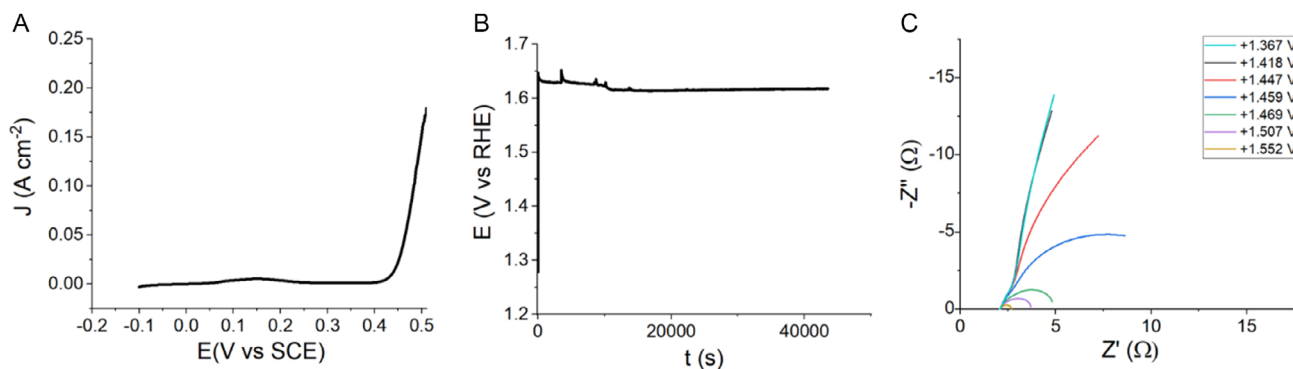


Figure 8. A) LSV recorded in 1 M KOH at the Grafoil electrode modified with Co60Ni20Fe20; B) stability test carried out in 1 M KOH by applying 10 mA cm^{-2} for 12 h; and C) EIS experiments carried out in 1 M KOH at different potentials (the values are reported with respect to RHE).

controlled by the oxygen evolution process facilitated by the electrocatalyst. Conversely, at potentials exceeding the onset potential, R3 becomes lower than R1 and R4, indicating that the overall electrochemical process rate is governed by resistance to charge transfer between Grafoil and LDH and in the electrolyte (Figure 8).

3. Conclusion

The transition toward renewable energy sources necessitates the storage of energy in chemical vectors, such as hydrogen. However, the high energy cost associated with the conversion of electrical to chemical energy remains a significant bottleneck in the realization of these energy storage devices. The development of efficient electrocatalysts for the oxygen evolution reaction is crucial to overcome this challenge and enable more sustainable energy systems.

In this study, we employed a chemometric experimental design strategy to systematically explore the composition–activity relationships of hydroxide-based electrocatalysts produced by electrochemical deposition. CV, XRD, and LSV analyses provided deeper insights into the electrocatalytic properties of the investigated materials: 1) Molar fractions of around 0.2 for Ni and Fe components allowed for high performance in terms of overpotential decrease. 2) Co component ensured reversible electrochemical behavior and enabled lower Tafel slope values. 3) The best electrocatalysts were identified in the region where the formation of a LDH phase was permitted.

Furthermore, the obtained data enabled us to derive predictive models that describe the material properties as a function of composition. The validity of these models was assessed by studying electrocatalysts with different compositions in comparison with those used for the fitting and by estimating the prediction error for the training points. These models offer valuable insights into the relationships between the electrocatalyst formulation and its OER performance, paving the way for the rational design of more performant and stable materials for energy conversion applications.

The efficient use of experimental resources through the chemometric approach can play a key role in accelerating the discovery and development of these advanced electrocatalysts. The findings of this study lay the groundwork for further optimization and scale-up of the OER electrocatalysts, ultimately contributing to the advancement of renewable energy technologies and the transition toward a sustainable energy future.

4. Experimental Section

Chemicals: Nickel (II) nitrate hexahydrate, cobalt (II) nitrate hexahydrate, and ethanol were purchased from Sigma–Aldrich. Potassium hydroxide was obtained from Merck. Iron (III) nitrate nonahydrate was bought from VWR chemicals. All the reagents were analytical reagent grade and used as received. The supporting electrolytes for the electrochemical experiments were 0.10 or 1.0 M KOH. The salt solutions were prepared with distilled water. Grafoil GTJ (Graphite > 99.8%) was used as the support and was purchased from VED (<https://www.ved.it>).

Apparatus: The electrochemical experiments were performed in a single compartment, three-electrode cell endowed with an aqueous saturated calomel electrode (SCE) as reference electrode, a Pt gauze as the counter

electrode, and a Grafoil (active area $1 \times 1 \text{ cm}^2$) sheet as the working electrode. The electrodes were connected to a CH Instrument Mod. 660^oC, controlled by a personal computer via CH Instrument software.

Powder XRD was performed by means of an X'Pert PANalytical diffractometer equipped with a copper source ($K\alpha$ radiation, $\lambda = 0.15418 \text{ nm}$), operating in reflection mode. The 2θ interval from 5° to 60° was explored (step of 0.066°) and counting time of 300 s/point) with a fast X'Celerator detector. The length of coherent domains perpendicular to 003 plane was calculated by Scherrer equation.

LDHs Electrodeposition: The LDH electrodepositions were carried out on Grafoil sheets. Preliminarily, the supports were rinsed in ethanol for 10 min and then dried to a constant weight. The LDH films were deposited on the conductive surface immersed into a freshly prepared solution, containing $\text{Ni}(\text{NO}_3)_2$ and/or $\text{Co}(\text{NO}_3)_2$ and/or $\text{Fe}(\text{NO}_3)_3$. The total concentration of metal ions was 0.03 M and the compositions of all deposition solutions are reported in Table S1, Supporting Information, and were planned by DOE. The LDH deposition was carried out by applying four CV segments between -0.1 and -1.2 V , versus SCE, at a scan rate of 40 mV s^{-1} . The modified electrodes are named CoXXNiYYFeZZ , where XX, YY, and ZZ are the cobalt, nickel and iron molar percentages in the electrochemical bath, respectively.

Electrochemical Characterization: The electrochemical behavior of the electrodes was studied by CV in a suitable potential window at 0.010 V s^{-1} scan rate in 0.1 M KOH. In each experiment, CV curves were continuously recorded until the cycles resulted superimposable.

Evaluation of OER Performances: The catalytic activity of the electrodes was investigated in 1.0 M KOH by linear LSV recording iR-corrected polarization curves at the scan rate of 0.010 V s^{-1} . This scan rate was slow enough to ensure a steady-state behavior at the electrode surface. The Tafel slope was extracted in this way: from the LSV responses a graphic was derived reporting the potential values as a function of the current logarithm; nearby the section where oxygen evolution occurs, a straight line was interpolated. Its slope represents the Tafel slope. The onset potential was calculated by using LSV. First of all, the current value was obtained from the minimum point nearby the section where oxygen evolution occurs, and nearby the same section a straight line was interpolated. Inserting in its equation the current value, the onset potential was obtained. EIS spectra were recorded in 1.0 M KOH with the frequency ranging from 0.1 and 10^5 Hz at an AC amplitude of 10 mV.

Design of Experiments, Data Presentation, and Elaboration: For three components, the experimental region is represented by a triangle where each vertex corresponds to an electrode modified with one pure component. The experimental design was based on a simplex-lattice ternary diagram with a variation in the proportion of each metal of 20%. In this way, 21 experimental points should have been investigated, but they were reduced to 20 because it was not possible to prepare a pure iron-based electrode with a useful response. The constraint of the model is given by the fact that the sum of component fractions must be equal to 1.^[28] The experimental ternary diagrams reported in the Section 3.2, 3.3, and 3.4 are plotted using the software Origin lab. The experimental surfaces have been obtained by dividing the area of the ternary diagram into triangles, whose vertices correspond to the points investigated (Table S1, Supporting Information and Figure 1). These triangles share a side and do not overlap. The experimental surfaces of each triangle were created from the plane passing through the three vertices. The experimental data were fitted using Sigmaplot 10.0.1 for model fitting to obtain the models that best describe the trend of parameters as a function of the variables. Depending on the response, the employed polynomial equations were quadratic or full cubic. The response surfaces were plotted using Origin lab.

Supporting Information

Supporting Information is available from the Wiley Online Library or from the author.

Conflict of Interest

The authors declare no conflict of interest.

Author Contributions

Isacco Guanlandi: Formal analysis (lead); Supervision (supporting); Writing—original draft (lead); Writing—review and editing (equal). **Elisa Musella:** Formal analysis (supporting); Investigation (equal); Writing—review and editing (equal). **Giulia Costa:** Data curation (equal); Investigation (equal); Writing—original draft (supporting); Writing—review and editing (supporting). **Massimo Gazzano:** Data curation (supporting); Formal analysis (supporting); Writing—original draft (supporting). **Erika Scavetta:** Funding acquisition (equal); Supervision (supporting); Writing—review and editing (supporting). **Sergio Zappoli:** Data curation (equal); Formal analysis (equal); Methodology (equal); Writing—original draft (supporting); Writing—review and editing (supporting). **Domenica Tonelli:** Funding acquisition (equal); Methodology (supporting); Supervision (lead); Writing—original draft (supporting); Writing—review and editing (equal).

Data Availability Statement

The data that support the findings of this study are available in the supplementary material of this article.

Keywords

experimental designs, layered double hydroxides, oxygen evolution reaction electrocatalysts, water splitting

Received: July 31, 2024
Revised: October 10, 2024
Published online:

- [1] L. She, G. Zhao, T. Ma, J. Chen, W. Sun, H. Pan *Adv. Funct. Mater.* **2022**, *32*, 1.
- [2] M. Yu, E. Budiayanto, H. Tüysüz, *Angew. Chem., Int. Ed.* **2022**, *61*, e202103824.
- [3] T. M. Gür, *Energy Environ. Sci.* **2018**, *11*, 2696.
- [4] I. Roger, M. A. Shipman, M. D. Symes, *Nat. Rev. Chem.* **2017**, *1*, 0003.
- [5] B. Dunn, H. Kamath, J. M. Tarascon, *Science* **2011**, *334*, 928.
- [6] Z. Cai, X. Bu, P. Wang, J. C. Ho, J. Yang, X. Wang, *J. Mater. Chem. A* **2019**, *7*, 5069.
- [7] L. Lv, Z. Yang, K. Chen, C. Wang, Y. Xiong, *Adv. Energy Mater.* **2019**, *9*, 1.
- [8] M. Tahir, L. Pan, F. Idrees, X. Zhang, X. L. Wang, J. Zou, Z. Lin, *Nano Energy* **2017**, *37*, 136.
- [9] R. Subbaraman, D. Tripkovic, K. C. Chang, D. Strmcnik, A. P. Paulikas, P. Hirunsit, M. Chan, J. Greeley, V. Stamenkovic, N. M. Markovic, *Nat. Mater.* **2012**, *11*, 550.
- [10] J. He, M. Wei, B. Li, Y. Kang, D. G. Evans, X. Duan, *Layer Double Hydroxides* **2006**, *119*, 89.
- [11] P. D. T. J. Meyer, H. W. R. J. Sauvage, *Layered Double Hydroxides* (Eds: X. Duan, D. G. Evans), Springer, Heidelberg **2006**.
- [12] A. I. Khan, D. O'Hare, *J. Mater. Chem.* **2002**, *12*, 3191.
- [13] Z. Li, J. Yang, R. Gao, S.-M. Xu, X. Kong, X. Hua, P. Zhao, H. Hao, D. O'Hare, Y. Zhao, *J. Phys. Chem. Lett.* **2024**, *15*, 2006.
- [14] Y. Vlamidis, E. Scavetta, M. Gazzano, D. Tonelli, *Electrochim. Acta* **2016**, *188*, 653.
- [15] F. Yang, K. Sliozberg, I. Sinev, H. Antoni, A. Bähr, K. Ollegott, W. Xia, J. Masa, W. Grünert, B. R. Cuenya, W. Schuhmann, M. Muhler, *ChemSusChem* **2017**, *10*, 156.
- [16] C. Zhengyang, B. Xiuming, W. Ping, C. H. Johnny, Y. Junhe, W. Xianying, *Mater. Chem. A* **2019**, *7*, 5069.
- [17] J. Wang, L. Wang, X. Chen, Y. Lu, W. Yang, *J. Solid State Electrochem.* **2015**, *19*, 1933.
- [18] X. Gao, X. Pan, X. Long, Z. Yi, *J. Electrochem. Soc.* **2017**, *164*, 3230.
- [19] S. D. Brown, T. B. Blank, S. T. Sum, L. G. Weyer, *Chemom. Anal. Chem.* **1994**, *66*, 315.
- [20] R. A. Olivero, J. M. Nocerino, S. N. Deming, *Handbook Environ. Chem.* **1995**, *2*, 73.
- [21] I. Gualandi, Y. Vlamidis, L. Mazzei, E. Musella, M. Giorgetti, M. Christian, V. Morandi, E. Scavetta, D. Tonelli, *ACS Appl. Nano Mater.* **2019**, *2*, 143.
- [22] E. Musella, I. Gualandi, M. Giorgetti, E. Scavetta, A. Rivalta, E. Venuti, F. Corticelli, M. Christian, V. Morandi, D. Tonelli, *Appl. Clay Sci.* **2021**, *202*, 105949.
- [23] E. Musella, I. Gualandi, E. Scavetta, M. Gazzano, A. Rivalta, E. Venuti, M. Christian, V. Morandi, D. Tonelli, *Chem. - Eur. J.* **2019**, *25*, 16301.
- [24] E. Musella, I. Gualandi, E. Scavetta, A. Rivalta, E. Venuti, M. Christian, V. Morandi, A. Mullaliu, M. Giorgetti, D. Tonelli, *J. Mater. Chem. A* **2019**, *7*, 11241.
- [25] R. Leardi, *Anal. Chim. Acta* **2009**, *652*, 161.
- [26] J. A. Cornell, *Experiments with Mixtures: Designs, Models, and the Analysis of Mixture Data*, 3rd ed, Wiley, New York **2002**.
- [27] R. H. Myers, D. C. Montgomery, C. M. Anderson-Cook, *Response Surface Methodology: Process And Product Optimization Using Designed Experiments*, 4th ed., Wiley, Hoboken, New Jersey **2016**.
- [28] a) H. Scheffé, *J. Royal Stat. Soc., Ser. B* **1958**, *20*, 344; b) H. Scheffé, *J. Royal Stat. Soc., B* **1965**, *25*, 235.
- [29] L. Trotochaud, S. L. Young, J. K. Ranney, S. W. Boettche, *J. Am. Chem. Soc.* **2014**, *136*, 6744.
- [30] M. Huang, C. Cao, L. Liu, W. Wei, Q.-L. Zhu, Z. Huang, *eScience* **2023**, *3*, 100118.
- [31] S. S. Jeon, P. W. Kang, M. Klingenhof, H. Lee, F. Dionigi, P. Strasser, *ACS Catal.* **2023**, *13*, 1186.
- [32] S. Zhou, Y. Liu, J. Li, Z. Liu, J. Shi, L. Fan, W. Cai, *Green Energy Environ.* **2022**, *9*, 1151.